RESEARCH ARTICLE Open Access

Spatiotemporal topological combs for robust high-dimensional information transmission

Dawei Liu[1†], Xingyuan Zhang[2†], Daijun Luo[1,3†], Huiming Wang[4], Zhirong Tao[5], Dana JiaShaner[1], Zhigang Peng[1], Zhensheng Tao[6], Qian Cao[1], Xiaoshi Zhang[7], Qiwen Zhan[2,8*] and Guangyu Fan[1,9*]

Abstract

Time-varying orbital angular momentum (OAM) beams are fascinating due to their rich physics and essentially unbounded degrees of freedom. Yet, despite this promise, their practical use in high-capacity communication has not been demonstrated. We introduce a spatiotemporal topological comb (ST-Comb) as a programmable information carrier in which digital data are encoded into a generalized spatiotemporal-topological state space, rather than into a single vortex beam or an OAM mode. The accessible states are defined by temporal slots, spatiotemporal phase winding, radial topology, coherent topological superpositions, and ST-CEP-dependent spectral fingerprints. A Hyper-DoF ST-Comb modulator programs these variables in the k_x-ω plane, while a self-referenced Guide-Star pulse enables coherent reconstruction relative to an intrinsic optical reference. In the present proof-of-concept, we demonstrate 154 mapped digital bits per wavepacket, recovered with 100% recognition accuracy under tested laboratory, phase-screen-equivalent turbulence, and 100 m outdoor field-trial conditions. The results chart a path toward reconfigurable ultrafast photonics, where programmable spatiotemporal-topological states provide a robust physical alphabet for high-dimensional optical interconnects.

†Dawei Liu, Xingyuan Zhang, Daijun Luo have contributed equally to this work.

*Correspondence:
Qiwen Zhan
zhanqiwen@westlake.edu.cn
Guangyu Fan
gfan@usst.edu.cn
[1] School of Optical-Electrical and Computer Engineering, University of Shanghai for Science and Technology, Shanghai 200093, China
[2] Zhejiang Key Laboratory of 3D Micro/Nano Fabrication and Characterization, Department of Electronic and Information Engineering, School of Engineering, Westlake University, Hangzhou, Zhejiang 310030, China
[3] Attosecond Quantum Physics Laboratory, Department of Physics, King's College London, London, UK
[4] Institute of Photonics, TU Wien, Gusshausstrasse 27/387, Vienna, Austria
[5] Karlsruhe Institute of Technology, Karlsruhe, Germany
[6] State Key Laboratory of Surface Physics, Key Laboratory of Micro and Nano Photonic Structures (MOE), Department of Physics, Fudan University, Shanghai 200433, China
[7] Yunnan University, Kunming, Yunnan 650500, China
[8] International Institute for Sustainability with Knotted Chiral Meta Matter (WPI-SKCM2), Hiroshima University, Higashihiroshima, Hiroshima 739-8526, Japan
[9] Department of Physics and Electronics, Yunnan Normal University, Kunming, Yunnan 650000, China

© The Author(s) 2026. **Open Access** This article is licensed under a Creative Commons Attribution 4.0 International License, which permits use, sharing, adaptation, distribution and reproduction in any medium or format, as long as you give appropriate credit to the original author(s) and the source, provide a link to the Creative Commons licence, and indicate if changes were made. The images or other third party material in this article are included in the article's Creative Commons licence, unless indicated otherwise in a credit line to the material. If material is not included in the article's Creative Commons licence and your intended use is not permitted by statutory regulation or exceeds the permitted use, you will need to obtain permission directly from the copyright holder. To view a copy of this licence, visit http://creativecommons.org/licenses/by/4.0/.

1 Introduction

Light beams carrying orbital angular momentum (OAM) have established a powerful degree of freedom beyond polarization and frequency, driving advances in high-capacity optical communications, optical manipulation, and quantum information processing [1–4]. Recently, the research frontier has shifted from static to time-varying OAM beams, which bring unprecedented degrees of freedom and reveal a profoundly rich physical landscape [5–7]. In these dynamic beams, the topological charge evolves continuously in time, inherently coupling spatial, temporal, and spectral degrees of freedom to generate a large and highly structured state space. This temporal modulation radically expands the Hilbert space of light beyond static encoding, offering tantalizing schemes for high-dimensional information multiplexing, while also raising fundamental questions on the conservation and transfer of angular momentum in time-dependent systems [8, 9]. Furthermore, experiments demonstrating the generation of extreme-ultraviolet beams with time-varying OAM have directly linked structured light to the attosecond scale [10–16]. Time-varying OAM generation has recently been extended to integrated photonic platforms, unlocking the potential for chip-scale multidimensional nonlinear optics [17] and the development of integrated optical vortex microcombs [18]. These breakthroughs underscore that time-varying OAM is not merely an extension of conventional singular optics, but a fundamentally new regime with immense potential for both fundamental physics and disruptive photonic technologies.

Despite its extraordinary promise, the real-world application of time-varying OAM is fundamentally bottlenecked by its inherent fragility, as inevitable spatiotemporal astigmatism easily fractures its delicately coupled topology, a vulnerability that can be further exacerbated by atmospheric turbulence [19, 20]. These effects increase crosstalk and reduce the reliability of state recognition. At the same time, practical channel capacity is constrained by the available bandwidth and signal-to-noise ratio [21–24]. A useful communication framework must therefore do more than generate time-varying OAM; it must define a recoverable state space, provide a robust coherent reference, and specify how encoded states are multiplexed, reconstructed, and decoded after propagation.

Here we propose a spatiotemporal topological comb (ST-Comb) framework for high-dimensional information transmission. Unlike previous studies centered on time-varying structured light and OAM dynamics, the present work uses the ST-Comb as a programmable spatiotemporal-topological information carrier, rather than as another vortex-beam geometry. Here, "topological" refers to the encoded and recovered global field identity, or topological fingerprint, defined not only by spatiotemporal phase winding but also by radial topology, coherent topological superpositions, and ST-CEP-dependent spectral features. This broader definition allows topological field structures to function as addressable symbols for high-dimensional information encoding. Using a Hyper-DoF ST-Comb modulator, we program these degrees of freedom across temporal sub-pulses and shift the resulting fingerprints away from the dominant low-frequency technical-noise band through a lock-in-inspired out-of-band encoding strategy [25]. A co-propagating Gaussian Guide-Star then serves as an intrinsic reference for self-referenced coherent demodulation. With this architecture, we experimentally demonstrate 154 mapped digital bits per wavepacket and recover the payload after laboratory free-space propagation, phase-screen-equivalent 1 km and 10 km turbulence tests, and a 100 m outdoor field trial at the Shanghai Astronomical Observatory.

2 Results

2.1 Concepts of ST-Comb and Optical Lock-In

We establish the concept of optical lock-in and introduce the spatiotemporal topological comb (ST-Comb) as a model system. In the time domain, the ST-Comb appears as a sequence of ultrafast sub-pulses (Fig. 1a), each carrying individually addressable topological modes. Previous work showed that 4*f* optical shapers generate time-varying OAM by preserving the spiral phase under 2D Fourier mapping [5, 7]. A direct mapping from the spectral domain to spatiotemporal topology, however, remained counterintuitive. Here, Hyper-DoF refers specifically to the programmable encoding dimensions of the ST-Comb, including sub-pulse amplitude, temporal delay, spatiotemporal topological charge, radial index, and the relative phase associated with ST-CEP. The electric field distribution of the generated comb is formulated as (Methods):

$$E(x,y,t)=\sum_{n} C_n A_n(x,y,t-t_n;\mu_n)\exp\{i[\omega_0 t+\varphi_{\text{ST-CEP}}(n)]\}, \tag{1}$$

Here, C_n denotes the target complex amplitude weight assigned to the n-th sub-pulse, A_n is the normalized spatiotemporal mode profile, and μ_n collects the controlled topological variables such as azimuthal charge ℓ and radial index p. The phase $\varphi_{\text{ST-CEP}}(n)$ is the spatiotemporal carrier-envelope phase offset of the sub-pulse. Modulating $\varphi_{\text{ST-CEP}}$ controls the spectral shift $\Delta\nu=\Delta\varphi/2\pi\tau$, where τ is the interval between sub-pulses. In the experiment, the target C_n values are prescribed by the designed pulse train and then pre-compensated using measured system response, including SLM phase response,

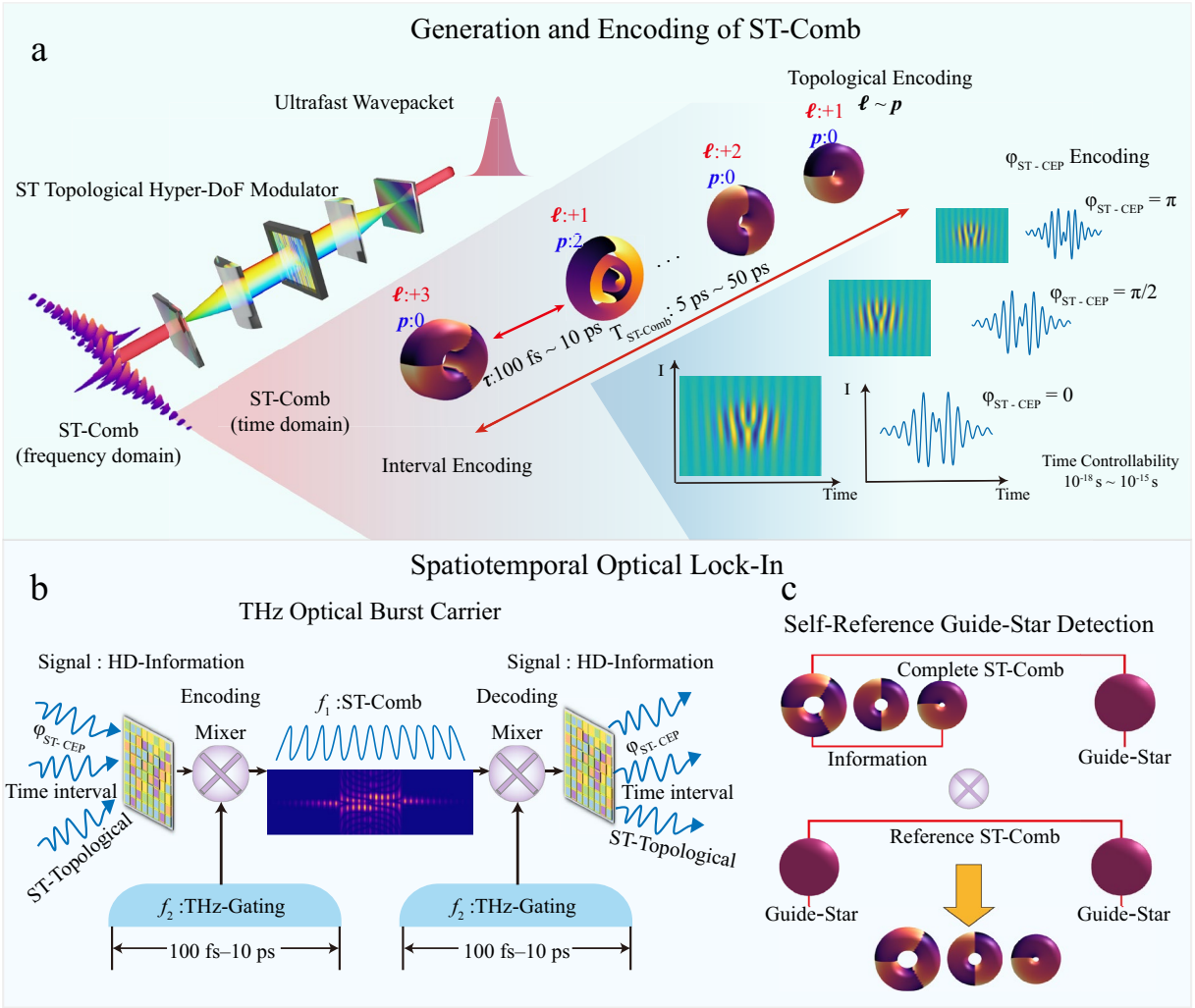


Fig. 1 Generation of the ST-Comb and spatiotemporal optical lock-in. **a** Formation and encoding. An ultrafast pulse is shaped by a spatiotemporal modulator into a sequence of spatiotemporal-topological sub-pulses. The fs-ps inter-pulse spacing corresponds to a THz-rate carrier. The topological modes (including radial index p and azimuthal index ℓ), temporal separation τ, and relative phase difference φ_{ST-CEP} of each sub-pulse can all be utilized for information encoding. **b** Spatiotemporal lock-in encoding. All spatiotemporal information is loaded onto a THz-burst carrier via the modulator, achieving spatiotemporal phase lock-in and heterodyning with an information-free Gaussian THz gating pulse retrieves the encoded spatiotemporal content. **c** Self-reference "Guide-Star" detection. The first sub-pulse is set as a Gaussian Guide-Star and temporally separated from the information-bearing sub-pulses. Subtracting the two-Gaussian reference ST-Comb calibrates the system transfer function, enabling Fourier-domain isolation and reconstruction of the spatiotemporal topological information

diffraction efficiency, input spectrum, optical throughput, and detector response (Supplementary Section 1).

Conventional lock-in detection improves weak-signal readout by referencing the signal to a known modulation channel and rejecting noise outside the detection bandwidth. Inspired by this principle, our optical implementation combines out-of-band spatiotemporal encoding with self-referenced coherent demodulation, rather than a literal electronic lock-in process. First, the femtosecond-to-picosecond sub-pulse spacing maps the encoded information onto ultrafast temporal and spectral fingerprints, shifting the useful signal away from the dominant low-frequency technical-noise band (Fig. 1b). Second, we introduce a self-referenced Guide-Star architecture, in which the first sub-pulse is kept Gaussian and temporally separated from the following information-bearing sub-pulses (Fig. 1c). This co-propagating Gaussian pulse serves as an intrinsic reference for spectral interferometry, allowing the relative amplitude and phase of the encoded sub-pulses to be reconstructed by

Fourier-domain filtering and inverse transformation of the reference–signal interference terms (Supplementary Section 2). Because the Guide-Star and the encoded sub-pulses originate from the same parent wavepacket and propagate along a common optical path, environmental phase drifts are largely common-mode and can be suppressed in the reconstructed relative field. Finally, propagation may distort the local intensity and phase distributions, and high-order spatiotemporal vortices may split into multiple lower-order singularities. However, in the tested propagation and turbulence conditions, such local rearrangements appear as a redistribution of topological charge within the reconstructed field, while the global net winding or topological fingerprint used for decoding remains preserved and identifiable (Supplementary Section 3).

2.2 Temporal and Spectral Properties of ST-CEP and ST-Comb

Manipulating the carrier-envelope phase (CEP)—the phase between the carrier wave and the pulse's intensity envelope enables sub-cycle waveform control, pushing light-matter interaction to its temporal limit and opening the door to PHz-rate information processing [26]. While recent pioneering studies have successfully extended the traditional CEP to control the spatial wavefront of single sub-cycle optical vortices [27], our work introduces a distinct macroscopic parameter: the spatiotemporal carrier-envelope phase (φ_{ST-CEP}). Unlike traditional CEP (φ_{CEP}), which dictates the absolute phase between the carrier wave and the intensity envelope within a single pulse, φ_{ST-CEP} defines the relative topological phase offset between adjacent sub-pulses within a picosecond-spaced pulse train. By modulating a single wavepacket into this pulse train, each sub-pulse carries the same absolute φ_{CEP}, while the independently tunable phase φ_{ST-CEP} is encoded into each sub-pulse through a spatiotemporal modulation scheme (Fig. 2a). Crucially, φ_{CEP} and φ_{ST-CEP} coexist without mutual interference; φ_{ST-CEP} alone governs the ST-Comb's spectral intensity distribution. This decoupling renders our encoding scheme insensitive to absolute CEP noise, allowing arbitrary spatiotemporal phase modulation without the need for complex CEP-stabilized laser sources.

In both the time and frequency domains, the ST-Comb displays a unique spatiotemporal topological structure. As shown in Fig. 2b, its temporal structure is two-scale. A short scale (100 fs–10 ps) sets the inter-pulse delay τ, and a long scale (5–50 ps) sets the total train duration. By Fourier duality, τ fixes the primary tooth spacing $\Delta\nu = 1/\tau$ in the sub-THz-THz range, while the finite train length introduces a secondary low-frequency spacing of 20–200 GHz. As an example, for an ST-Comb with topological number [1; 1; 1], the field can be modeled as the convolution of a Gaussian pulse train with a spatiotemporal-topological wavepacket (Supplementary Section 4), showing that the time-domain signal is jointly shaped by the Gaussian sequence and the ST-topological envelope. In the spectral domain (Fig. 2c), the spectrum factorizes into the product of an optical frequency comb and a STOV spectrum. Fine comb lines arise from the long-period (5–50 ps) train, and the THz-scale envelope is fixed by τ, yielding a composite spectrum spanning orders of magnitude.

2.3 Parameter-Space Encoding of High-Dimensional Information

To construct an information space, we organize the ST-Comb degrees of freedom into a programmable parameter space (Fig. 3a). The vertical coordinate represents the spatiotemporal topological state, the radial coordinate represents inter-pulse spacing, and the polar angle represents ST-CEP. Each point can be further indexed by the radial mode p. Figure 3b-d show experimental and simulated control over these degrees of freedom. In the angular-topology dimension (Fig. 3b), we realize ST-Combs whose ℓ values evolve linearly or aperiodically in time, producing distinguishable topology-time trajectories (Supplementary Section 5). ST-CEP control produces different spectral fingerprints while preserving the same temporal-slot structure (Fig. 3c), and radial-mode control adds another topological index (Fig. 3d). Thus the ST-Comb state space used here is broader than a single OAM value: it includes temporal position, azimuthal topology, radial topology, coherent superposition, and phase-dependent spectral fingerprints (Supplementary Section 6).

The coupling between time and frequency resources in physical systems is rooted in Fourier-transform duality. This duality enforces a dynamic constraint mechanism on the distribution of information across time and frequency domains, ensuring that the allocation of resources in one domain directly influences and limits

(See figure on next page.)

Fig. 2 Temporal and Spectral properties of ST-CEP and ST-Comb. **a** Time- and frequency-domain waveforms under two ST-CEP settings. Tuning the ST-CEP enables THz-scale spectral sweeping. **b** ST-Comb in the time domain. The comb forms a pulse train with 100 fs–10 ps inter-pulse spacing and a total burst duration of 5–50 ps; adjusting ST-CEP translates the electromagnetic-field envelope within the burst. **c** ST-Comb in the frequency domain. The inter-pulse spacing τ sets the comb-line spacing in the sub-THz-THz band, yielding a dense comb and long-period modulation of the pulse train introduces an additional low-frequency spacing of 20–200 GHz

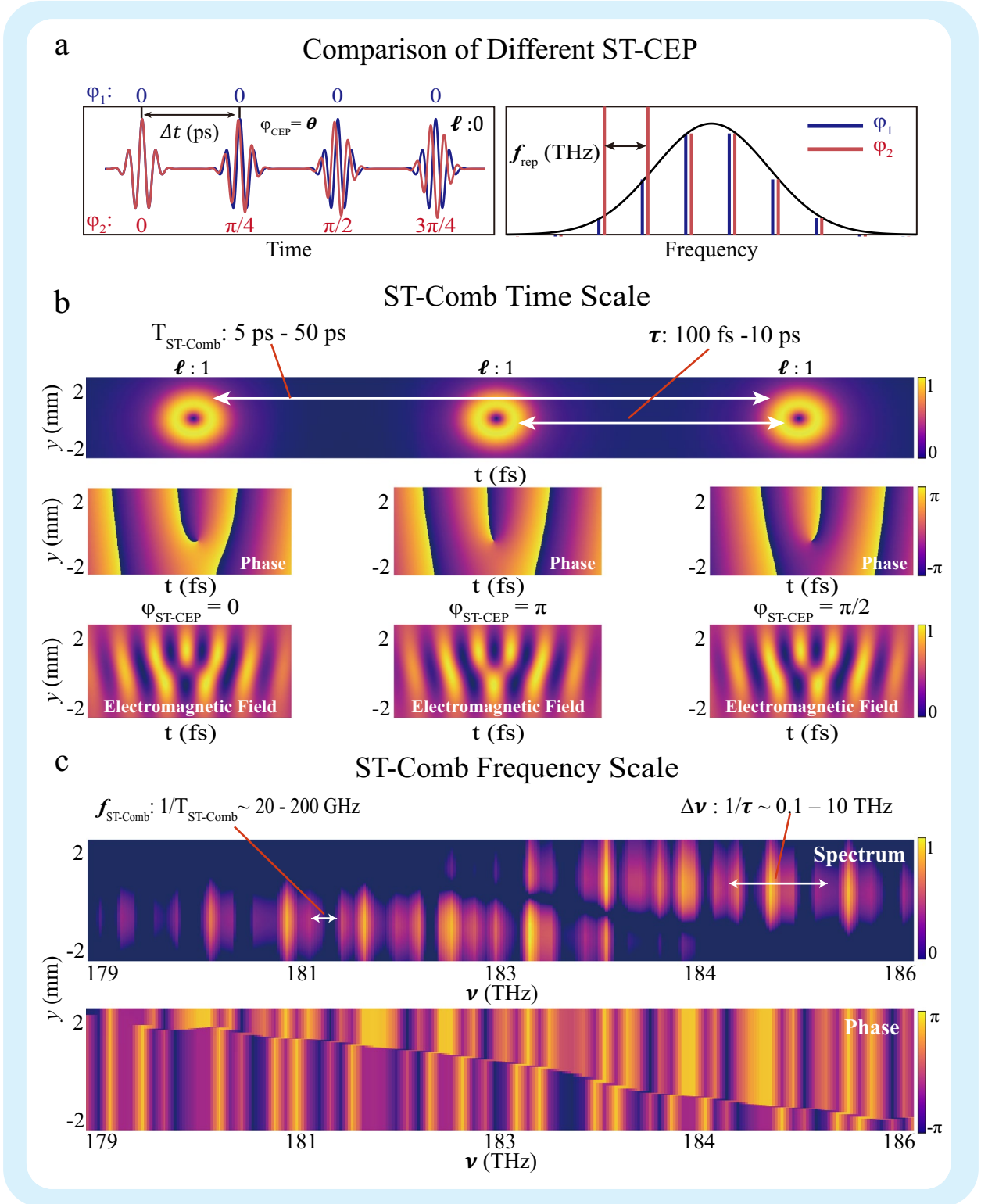


Fig. 2 (See legend on previous page.)

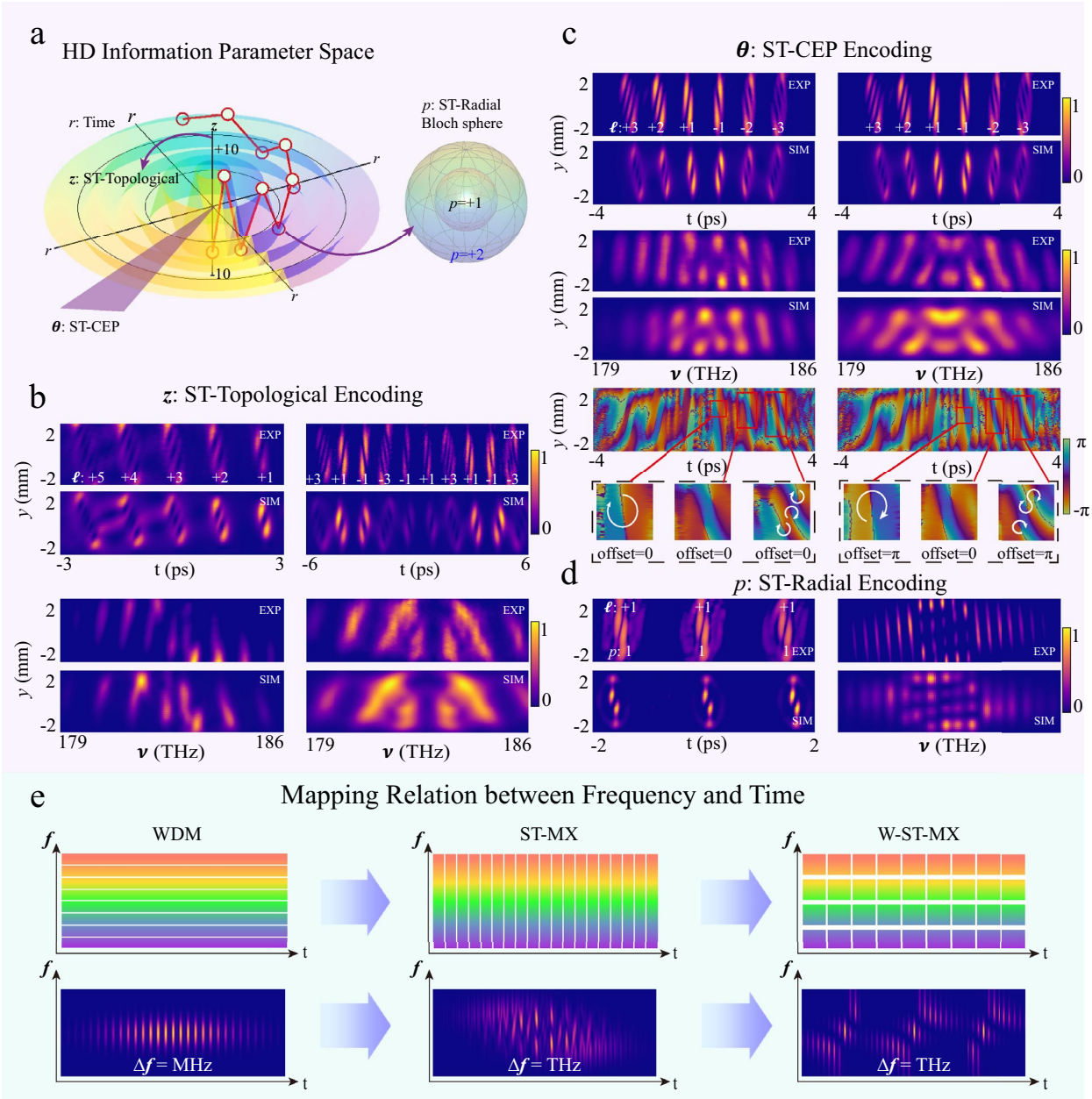


Fig. 3 Degrees of freedom for high-dimensional manipulation of the ST-Comb and mapping relation from time-frequency resources. **a** Schematic of the high-dimensional information space of the ST-Comb. **b** Spatiotemporal topological encoding (information-space *z*-axis). Examples showing ST-Combs with linear and nonlinear mappings between time and topological charge ℓ. **c** ST-CEP control (parameter-space θ-axis). Varying the spatiotemporal carrier-envelope phase φ_{ST-CEP} preserves the time-domain waveform while inducing pronounced spectral differences. **d** Radial topological *p* control. ST-Combs combining ℓ with the radial index *p*. **e** Mapping relation from frequency to time across three modes: frequency multiplexing, spatiotemporal multiplexing, and hybrid frequency-spatiotemporal multiplexing

the characteristics of the other, as quantitatively mapped by the Wigner distribution (Fig. 3e). However, developing an optimal allocation framework that satisfies these physical constraints remains a critical theoretical challenge in advancing communication technologies [28]. Current information multiplexing schemes primarily focus on the frequency domain, such as WDM [29]. The time domain has been increasingly overlooked, as traditional solitons lack programmable time structures, making it challenging to directly encode information in their temporal degrees of freedom. The ST-Comb enables discrete time-domain partitioning at fs-ps resolution,

unlocking ultrafast temporal-structure modulation and high-dimensional information encoding via programmable spatiotemporal topologies.

2.4 Multiplexing and Demultiplexing of ST-Comb

Prior work has shown that propagation can induce intrinsic splitting and mode conversion in spatiotemporal topology [19, 20]. We therefore distinguish the local field morphology from the global topological identity used for information decoding. During propagation, local intensity and phase structures may distort, and high-order spatiotemporal vortices may split into multiple lower-order singularities. In the free-space and phase-screen conditions tested here, however, this splitting appears as a redistribution of local topological charge within the reconstructed field, while the global net winding or topological fingerprint remains identifiable after Guide-Star reconstruction. This recoverable fingerprint motivates the multiplexing-demultiplexing architecture shown in Fig. 4. At the transmitter, multiple temporal slots are synthesized by the SLM mask, with each slot assigned a programmable amplitude, delay, topological basis state or superposition, radial index, and phase/ST-CEP offset. To quantify the addressable state space, we define N_t as the number of information-bearing temporal slots, N_ℓ as the number of resolvable azimuthal or topological basis modes, N_p as the number of radial modes, N_{CEP} as the number of ST-CEP states, and N_ϕ as the number of discretized relative-phase states when phase-coded superpositions are used (Supplementary Section 7). For single-mode encoding, each temporal slot selects one state from $N_\ell N_p N_{\mathrm{CEP}}$ available states, giving $(N_\ell N_p N_{\mathrm{CEP}})^{N_t}$ wavepacket states, or $N_t \log_2(N_\ell N_p N_{\mathrm{CEP}})$ bits. For binary topological-superposition encoding, each slot is represented by a binary mask over $N_b = N_\ell N_p$ selectable modes, corresponding to 2^{N_b} possible labels, or N_b mapped bits per slot. In our 154-bit demonstration, $N_t = 11$ information-bearing slots and $N_b = 14$ selectable topological modes are used, yielding $11 \times 14 = 154$ mapped digital bits per wavepacket. The Gaussian Guide-Star is used only as a reference and is not counted as payload. As a scalability example, 40 temporal slots with 20 selectable modes per slot give $(2^{20})^{40} = 2^{800}$, corresponding to an 800-bit state label (Supplementary Section 8). The physical limits of this scaling, including SLM sampling, temporal-window size, ST-CEP resolution, detection dynamic range, and crosstalk, are discussed in Supplementary Section 14.

The receiver performs demultiplexing in three steps: coherent waveform reconstruction, temporal slicing, and topological-state recognition. First, the Guide-Star spectral interferogram is Fourier transformed to recover the complex waveform. The reconstructed wavepacket is then separated into temporal slots according to the known inter-pulse delays (Fig. 4b). Finally, ST-Net is applied to each temporal slice to recognize the topological superposition or spectral fingerprint and map the recognized state back to the corresponding bit sequence (Fig. 4c). We therefore use time-demultiplexing to describe the physical separation of temporal slots, and state recognition or decoding to describe the machine-learning-assisted identification of the encoded topological state. The trained model achieved 100% classification accuracy on the tested 1000 randomly generated ST-Comb samples (Fig. 4e), while repeatability was evaluated over 100 repeated measurements of identical configurations (Fig. 4d).

2.5 High-Robustness Information Transmission

We demonstrate ST-Comb information transmission under turbulent and outdoor free-space conditions, with the robustness verification summarized in Fig. 5. After propagation, the received wavepacket is not decoded from a distorted instantaneous intensity image. Instead, Guide-Star coherent reconstruction retrieves the relative complex field, from which ST-Net identifies the temporal slots and their spatiotemporal-topological fingerprints (Supplementary Sections 9 and 10). The physical origin of the robustness is therefore revealed by the different responses of the local field morphology and the global encoded fingerprint. Atmospheric turbulence can induce beam wander, spatially dependent phase distortion, modal coupling, and envelope fragmentation, leading to a reduced conventional field fidelity F_{field}. However, the information carried by the ST-Comb is distributed across a coherent temporal-spectral structure and a Guide-Star-referenced topological state space, rather than being confined to the local transverse profile. As shown in Fig. 5b,c, F_{field} decreases with increasing turbulence strength, whereas the normalized fingerprint metric $K_{\mathrm{atmo}}/K_{\mathrm{ideal}}$ remains close to unity over the tested range (Supplementary Section 12). This contrast shows that the ST-Comb transforms turbulence-sensitive local waveform information into a recoverable spectro-topological identity, which remains identifiable from weak-fluctuation outdoor conditions to strong phase-screen-equivalent perturbations.

We further validated this mechanism in both real and controlled turbulent channels. A proof-of-principle outdoor free-space transmission experiment was performed over a 100 m direct-transmission path at the Shanghai Astronomical Observatory (Fig. 5d). As shown in Fig. 5e, the recovered ST-Comb states remain well separated for both single-topological-state and topological-superposition-state datasets, enabling high-fidelity outdoor

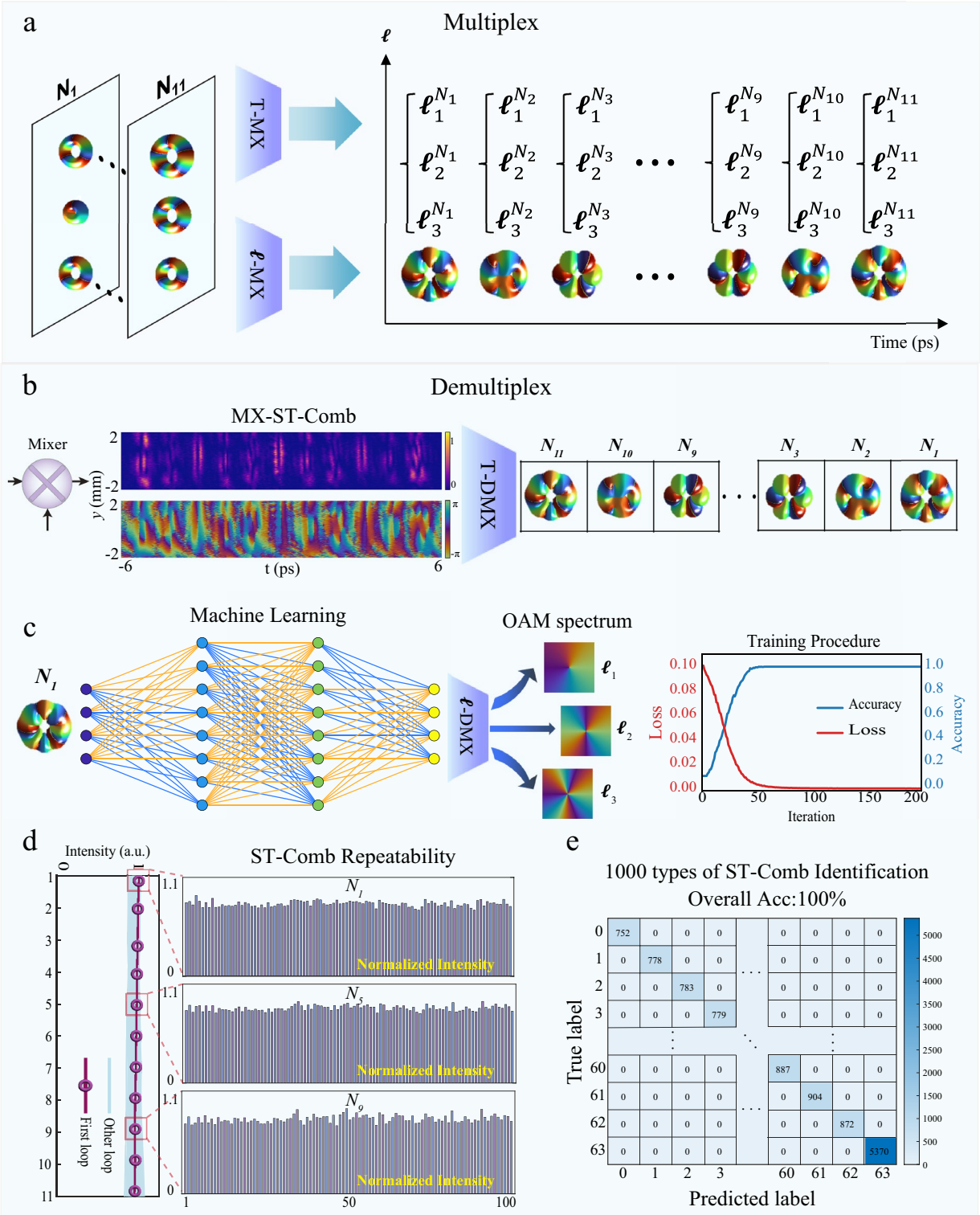


Fig. 4 Multiplexing-Demultiplexing Mechanism of ST-Comb. **a** Multiplexing process, femtosecond pulses undergo time multiplexing and spatiotemporal topological multiplexing to form hybrid-state ST-Comb. **b** Time demultiplexing process, after coherent decoding hybrid-state ST-Combs undergo time demultiplexing to isolate individual sub-pulses. **c** Topological-state recognition, time-demultiplexed sub-pulses are fed into ST-Net to recover the encoded topological information. **d** Repeatability demonstration, intensity stability results from 100 repetitions of identical ST-Comb configurations. **e** Experimental measurement of 1000 distinct ST-Combs achieves 100% recognition accuracy

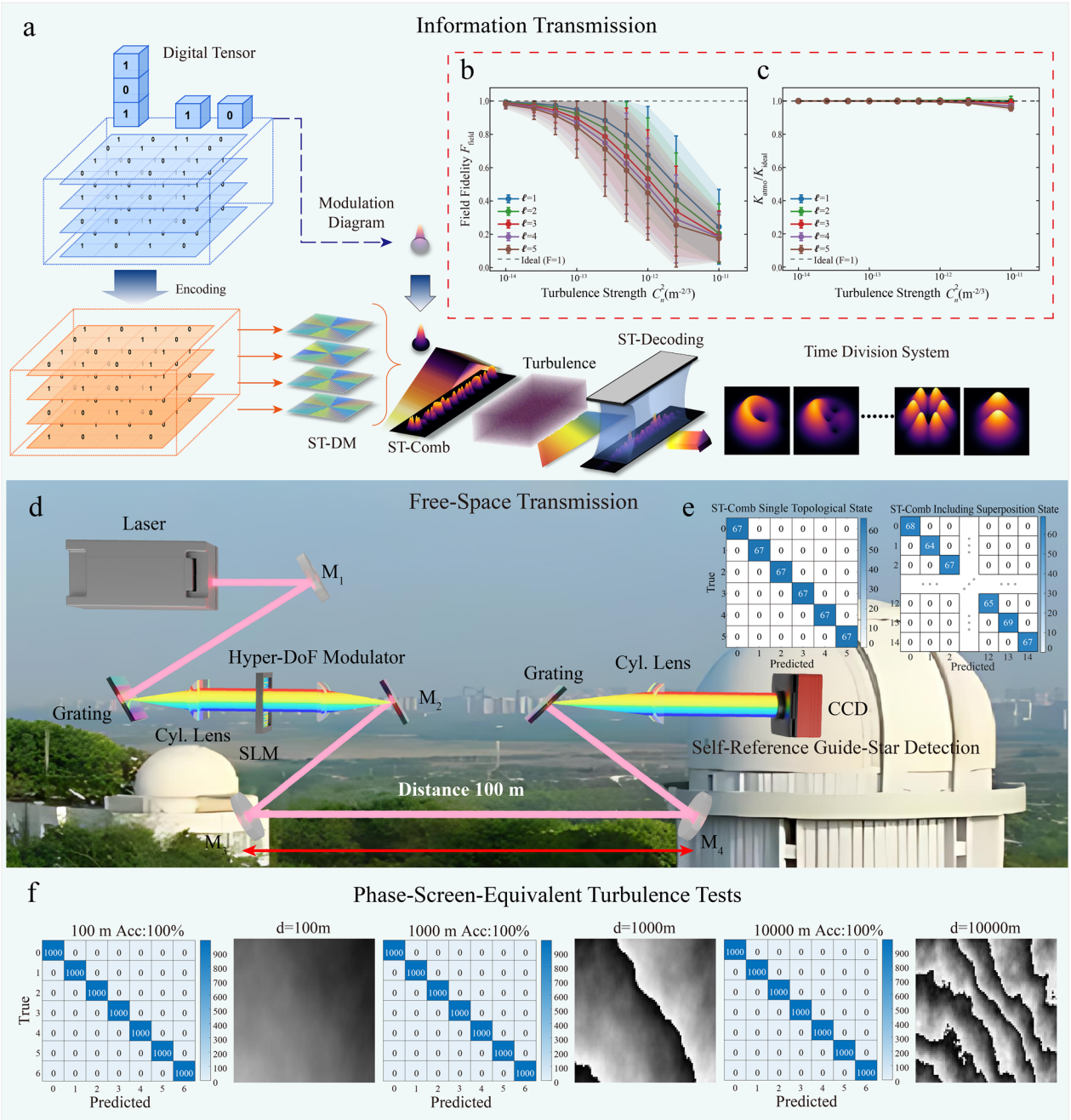


Fig. 5 ST-Comb information transmission with outdoor and phase-screen-equivalent turbulence tests. **a** Encoding-to-decoding workflow: digital payloads are mapped onto ST-Comb states, transmitted, reconstructed by self-referenced Guide-Star detection, temporally sliced, and decoded by ST-Net. **b** Field fidelity F_{field} versus turbulence strength C_n^2 under phase-screen propagation. **c** Normalized Schmidt-number ratio K_{atmo}/K_{ideal} under the same conditions, indicating that the global spectro-topological fingerprint remains recoverable. **d** Real 100 m outdoor direct-transmission field trial at the Shanghai Astronomical Observatory. **e** Recognition results for the 100 m outdoor field trial, including single-topological-state and topological-superposition-state ST-Combs. **f** Phase-screen-equivalent turbulence tests for equivalent propagation lengths of 100 m, 1000 m, and 10,000 m; these are not physical outdoor links

information recovery under the locally logged meteorological conditions and estimated weak-turbulence range summarized in Supplementary Table S2. To probe stronger accumulated wavefront perturbations, we introduced phase-screen-equivalent turbulence conditions corresponding to 100 m, 1 km, and 10 km propagation

cases into the same encoding–reconstruction–recognition pipeline (Fig. 5f and Supplementary Section 11). Across the evaluated outdoor and phase-screen-equivalent datasets, the encoded states were recovered without observed classification errors, with the dataset statistics and confidence analysis provided in Supplementary Section 10. Together, these results show that ST-Comb robustness does not require the local waveform to remain intact; it arises from encoding the payload into a self-referenced global spatiotemporal-topological fingerprint that remains recoverable after propagation.

3 Discussions

In this work, we introduce the ST-Comb as a programmable spatiotemporal-topological information framework for high-dimensional optical encoding and transmission. Rather than relying on a conventional electronic lock-in process, the architecture combines lock-in-inspired out-of-band encoding with self-referenced coherent demodulation. Information is mapped onto ultrafast temporal and spectral fingerprints, which are shifted away from the dominant low-frequency technical-noise band, while a co-propagating Gaussian GuideStar provides an intrinsic reference for reconstructing the relative amplitude and phase of the encoded sub-pulses. This combination enables robust recovery of high-dimensional payloads after laboratory free-space propagation, phase-screen-equivalent turbulence tests, and outdoor field transmission.

It is worth noting the conceptual parallels between our approach and recent breakthroughs in on-chip topological frequency combs [30, 31]. While both systems exploit comb-like spectral structures and topological concepts, their physical origins and protection mechanisms are distinct. On-chip topological combs rely on photonic band topology to protect edge-state solitons against fabrication disorder. In contrast, the ST-Comb reported here is rooted in programmable singular and spatiotemporal field topology. Its robustness does not arise from photonic band topology, but from the recoverability of global spatiotemporal-topological fingerprints after self-referenced coherent reconstruction. These fingerprints include spatiotemporal phase winding, radial topology, coherent topological superpositions, and ST-CEP-dependent spectral structures, and they serve as the addressable physical alphabet for information encoding and decoding. This distinction highlights how topological concepts can be used not only to stabilize photonic hardware, but also to enhance the resilience of information carriers in free-space optical channels.

Beyond robustness, the ST-Comb provides a scalable route to high-dimensional optical state engineering. Using a Hyper-DoF ST-Comb modulator, we program the encoding dimensions available in the present implementation, including sub-pulse amplitude, temporal delay, spatiotemporal topological charge, radial index, and the relative phase associated with ST-CEP. These degrees of freedom define a large combinatorial state space in which each temporal slot can carry a programmable topological fingerprint. Sub-pulse intensities, higher-order radial indices, and relative phases between superposed states provide additional state dimensions, offering substantial headroom for further scaling of payload density and state labeling. More broadly, the ability to program and recover such spatiotemporal-topological wavepackets may provide new opportunities for ultrafast waveform control, high-dimensional nonlinear optics [32], and extensions toward extreme-ultraviolet structured light and frequency-comb platforms [10, 33].

From an implementation perspective, the ST-Comb architecture is intrinsically scalable and compatible with emerging photonic platforms. It integrates naturally with on-chip frequency combs [34, 35], high-speed modulators [36, 37], programmable active metasurfaces [38], and active optical phased arrays [39, 40]. These technologies provide the hardware basis for ultrafast, high-capacity, and energy-efficient optical communication and computing (Supplementary Section 13). Although the present work focuses on scalar spatiotemporal topology, future ST-Combs could incorporate vectorial STOVs, vector beams, and polarization-structured states. Polarization would then provide an additional encoding dimension, further expanding the accessible state space for high-dimensional classical communication, mode-division multiplexing, and quantum-key-distribution-inspired protocols. Furthermore, the proposed framework promises to reshape a broad spectrum of photonic disciplines. With high-fidelity control over programmable spatiotemporal degrees of freedom, it can fuel breakthroughs in optical computing architectures [41, 42], accelerate the emergence of photonic artificial intelligence [43, 44], and open pathways to reconfigurable, ultra-high-dimensional light-field processors. Together, these capabilities point to a tangible trajectory from laboratory proof-of-concept to chip-scale platforms for future reconfigurable ultrafast photonics.

4 Methods

4.1 Experimental Setup

All experiments were performed using a Yb-based femtosecond laser operating at a 1 kHz repetition rate (central wavelength 1030 nm; spectral FWHM $\approx$ 20 nm; transform-limited pulse duration $\approx$ 170 fs). It is imperative to use a broadband femtosecond source rather than a continuous-wave (CW) or quasi-CW laser. The generation of the ST-Comb relies on the mapping from

the spatial-frequency domain (k_x, ω) to the space-time domain (x, t). This two-dimensional mapping fundamentally requires angularly dispersing a broad spectrum (ω) to synthesize ultrafast temporal sub-pulses. Moreover, the initial spectral bandwidth dictates the shortest achievable sub-pulse duration, which in turn establishes the maximum temporal encoding density (the comb tooth resolution).

The output beam was divided by a dielectric beam splitter. In one output arm, a folded two-dimensional spatiotemporal pulse modulator was used to imprint user-defined complex amplitude and phase profiles onto the pulse. The modulator consisted of three cascaded elements: (i) a reflective diffraction grating (1200 lines/mm) to angularly disperse the broadband spectrum; (ii) a cylindrical lens ($f = 200$ mm, with its axis parallel to the grating grooves) to focus the dispersed spectrum along the x-axis, and (iii) a phase-only reflective spatial light modulator (HOLOEYE GAEA) positioned at the Fourier plane. A precalculated phase-only holographic pattern encoding the desired complex transmittance was uploaded to the SLM, producing a spatiotemporal optical frequency comb in which each sub-pulse carried a programmable topological charge (Supplementary Section 1).

4.2 Mathematical Formulation of the ST-Comb

A spatiotemporal optical vortex comb (ST-Comb) can be synthesized by coherently superposing optical-field degrees of freedom (DoF) in both space and time. This process yields a train of structured wave packets with tightly coupled spatiotemporal vortex properties. Such packets are generally nonseparable, meaning the field cannot be expressed as a simple product of a spatial mode $L(\mathbf{r})$ and a temporal envelope $T(t)$, i.e., $L(\mathbf{r})T(t)$. The electric field can be written as

$$E(x,y,t) = \sum_n C_n A_n(x,y,t-t_n;\mu_n) \exp\left[i\left(\omega_0 t + \varphi_{\text{ST-CEP}}(n)\right)\right], \tag{2}$$

where $A_n(x,y,t-t_n;\mu_n)$ denotes the n-th spatiotemporal mode, C_n is the target complex weighting coefficient, ω_0 is the carrier frequency, and $\varphi_{\text{ST-CEP}}(n)$ is the spatiotemporal carrier-envelope phase of the n-th sub-pulse. The coefficient C_n is analytically prescribed from the desired pulse train, for example an equal-amplitude or deliberately weighted sequence, and the displayed SLM mask is calibrated to compensate the measured phase response, diffraction efficiency, spectral envelope, optical throughput, and detector response.

Recent advances enable the use of pulse trains in combination with a 4*f* pulse shaper to preserve helical phase in the two-dimensional Fourier domain. The resulting topological pulse train can be modeled as the convolution of a complex spatial amplitude distribution with a periodic Dirac comb along the time axis:

$$E(x_2,y_2,t) = G'(y_2) \sum_{n=-\infty}^{\infty} C_n(-i)^{\ell_n} \exp(-i\ell_n\varphi)\mathcal{H}_{\ell_n}[\cdot]e^{-R^2W} * \delta\left(t - \frac{n\varepsilon}{2\pi}\right), \tag{3}$$

where $G'(y_2)$ is the envelope along y (typically Gaussian), $\mathcal{H}_{\ell_n}[\cdot]$ denotes the Hankel transform, ℓ_n is the topological charge of the n-th sub-pulse, and ε is the temporal spacing of the pulse train. When spatial dispersion in the propagation medium is negligible, the space-time Dirac impulses simplify to $\delta\{t - n\varepsilon/2\pi, x\}$.

The fundamental principle underpinning the ST-Comb is the conservation of angular momentum under the mapping from the spatial-frequency domain (k_x, ω) to the space-time domain (x, t). By expanding the field in frequency and applying quasi-periodic complex-amplitude modulation in the spatial-frequency plane, we introduce controlled spatial-frequency couplings, thereby enabling precise tailoring of the topology-time manifold. Additional phase-encoding strategies can further enrich the complexity of the generated topological field structures.

To reveal the topology-time relationship, the field in Eq. (2) is projected onto the angular-momentum and temporal axes to obtain an ℓ-t distribution, analogous to the ω-t Wigner representation in ultrafast optics. In this map, C_n specifies the designed amplitude and phase weight of each sub-pulse, while periodic spectral modulation produces a pulse train with a well-defined temporal period. Because diffraction efficiency and system throughput are not perfectly uniform, the practical values of C_n are verified by Guide-Star reconstruction and adjusted through a measured transfer-function calibration rather than by a separate iterative optimization for every encoded state.

Expanding the control space of the vortex train reveals a correspondence between the temporal diffraction order n_t and the angular-momentum order n_ℓ. The topological phase factor $\exp(-i\ell_n\phi)$ and the temporal displacement $\delta(t - n\epsilon/2\pi)$ are coupled through the spatiotemporal diffraction index n. Although this coupling may appear restrictive, the pulse-shaping geometry allows the angular-momentum–time distribution to occupy a high-dimensional ℓ-t manifold rather than a single trajectory. The accessible encoding space is therefore defined by the resolvable temporal slots and by the topological, radial, and phase states that can be assigned to each slot. Its practical size is limited by the laser bandwidth, SLM

sampling, temporal detection window, dynamic range, and reconstruction fidelity.

4.3 Self-Reference Guide-Star Architecture

To reconstruct the complete temporal electric field of the ST-Comb, we employ a self-referenced "Guide-Star" scheme. In the time domain, the ST-Comb consists of a sequence of ultrafast sub-pulses. We fix the first sub-pulse as a Gaussian wave packet with a known spectral phase. This pulse acts as an intrinsic reference signal and co-propagates with all subsequent information-bearing sub-pulses, forming the signal ST-Comb. The resulting spectrum is equivalent to that of a Gaussian reference pulse interfering with the information-carrying pulses.

In practice, we generate a reference ST-Comb composed of two Gaussian sub-pulses, producing spectral interference fringes analogous to those formed by two Gaussian pulses. The spectra of the reference ST-Comb and the signal ST-Comb are Fourier-transformed along the spectral axis. From the transformed data, we isolate the non-zero-frequency sideband–corresponding to the cross-spectral term between the reference and the signal ST-Combs–while suppressing the DC and mirror terms. Applying an inverse Fourier transform to the filtered sideband yields the complex spectral amplitude of the signal field relative to the reference ST-Comb. The amplitude spectrum of the signal is obtained from the modulus ratio between the signal and reference complex spectra, whereas the spectral phase is retrieved from the phase difference between their cross terms. By zero-padding the complex spectrum symmetrically and Fourier-transforming it back into the time domain, we recover the full temporal profile of the optical field, including both amplitude and phase.

Because the reference and signal pulses share an identical optical path, their relative phase is inherently immune to the drift and noise typical of conventional dual-arm interferometers, eliminating the need for an external reference channel in direct spectral interferometry. The single-path geometry intrinsically suppresses common-mode noise, while the topological invariance of the encoded states ensures that their core features remain stable even under strong turbulence. This combination of self-referencing and topological robustness enables phase-stable, high-fidelity measurement of the complete ST-Comb waveform, making the method particularly well suited for free-space optical links operating in complex and dynamic environments.

Supplementary Information

The online version contains supplementary material available at https://doi.org/10.1186/s43593-026-00145-w.

Supplementary Material 1.

Acknowledgements

The authors gratefully acknowledge the Sheshan Station of Shanghai Astronomical Observatory, Chinese Academy of Sciences, for providing experimental support and site assistance during the outdoor field trial.

Author Contributions

Dawei Liu (D.W.L.), Daijun Luo (D.J.L.) and Guangyu Fan (G.Y.F.) conceived the original idea and initiated the project. Dawei Liu (D.W.L.) designed and performed the experiments. Xingyuan Zhang (X.Y.Z.) contributed to the theoretical model and analysis. Dawei Liu (D.W.L.), Xingyuan Zhang (X.Y.Z.), Guangyu Fan (G.Y.F.) and Qiwen Zhan (Q.W.Z.) analysed the data and wrote the manuscript. Daijun Luo (D.J.L.), Huiming Wang (H.M.W.), Zhirong Tao (Z.R.T.), Dana JiaShaner (D.J.), Zhigang Peng (Z.G.P.), Zhensheng Tao (Z.S.T.), Qian Cao (Q.C.) and Xiaoshi Zhang (X.S.Z.) contributed to discussion and manuscript improvement. All authors discussed the results and approved the final manuscript.

Funding

This work was supported by National Key Research and Development Program of China (Grant No. 2025YFF0515101, [Q.Z.]), National Natural Science Foundation of China (12374318 [G.F.], Z-2025-302-053 [G.F.], 12434012 [Q.Z.], 62535013 [Q.Z.], 12450407 [Z.T.], 12274091 [Z.T.], 12474336 [Q.C.]), National Key Research and Development Program of China (Grant No. 2021YFA1400200 [Z.T.]), Science and Technology Commission of Shanghai Municipality (22JC1400200 [Z.T.], 24JD1402600 [Q.Z.], 24QA2705800 [Q.C.]), Key Project of Westlake Institute for Optoelectronics (Grant No. 2023GD007 [Q.Z.]).

Data Availability

The data that support the findings of this study are available from the corresponding author upon reasonable request.

Declarations

Competing Interests

The authors declare that they have no competing interests.

Received: 8 April 2026 Revised: 1 September 2026 Accepted: 4 September 2026
Published online: 30 October 2026

References

1. J. Wang, J.-Y. Yang, I.M. Fazal, N. Ahmed, Y. Yan, H. Huang, Y. Ren, Y. Yue, S. Dolinar, M. Tur, A.E. Willner, Terabit free-space data transmission employing orbital angular momentum multiplexing. Nat. Photonics **6**, 488–496 (2012)
2. N. Bozinovic, Y. Yue, Y. Ren, M. Tur, P. Kristensen, H. Huang, A.E. Willner, S. Ramachandran, Terabit-scale orbital angular momentum mode division multiplexing in fibers. Science **340**, 1545–1548 (2013)
3. R.C. Devlin, A. Ambrosio, N.A. Rubin, J.P.B. Mueller, F. Capasso, Arbitrary spin-to-orbital angular momentum conversion of light. Science **358**(6365), 896–901 (2017)
4. Y. Shen et al., Optical vortices 30 years on: OAM manipulation from topological charge to multiple singularities. Light Sci. Appl. **8**, 90 (2019)
5. A. Chong, C. Wan, J. Chen, Q. Zhan, Generation of spatiotemporal optical vortices with controllable transverse orbital angular momentum. Nat. Photonics **14**(6), 350–354 (2020)
6. M. Piccardo, M. de Oliveira, V.R. Policht, M. Russo, B. Ardini, M. Corti, G. Valentini, J. Vieira, C. Manzoni, G. Cerullo, A. Ambrosio, Broadband control of topological–spectral correlations in space–time beams. Nat. Photonics **17**, 822–828 (2023)

7. C. Wan, Q. Cao, J. Chen, A. Chong, Q. Zhan, Toroidal vortices of light. Nat. Photonics **16**(7), 519–522 (2022)
8. G. Ruffato, Non-destructive OAM measurement via light-matter interaction. Light Sci. Appl. **11**(1), 55 (2022)
9. G. He, Y. Zheng, C. Zhou, S. Li, Z. Shi, Y. Deng, Z.-K. Zhou, Multiplexed manipulation of orbital angular momentum and wavelength in metasurfaces based on arbitrary complex-amplitude control. Light Sci. Appl. **13**(1), 98 (2024)
10. L. Rego, K.M. Dorney, N.J. Brooks, Q.L. Nguyen, C.-T. Liao, J.S. Román, D.E. Couch, A. Liu, E. Pisanty, M. Lewenstein et al., Generation of extreme-ultraviolet beams with time-varying orbital angular momentum. Science **364**(6447), eaaw9486 (2019)
11. Y. Fang, S. Lu, Y. Liu, Controlling photon transverse orbital angular momentum in high harmonic generation. Phys. Rev. Lett. **127**(27), 273901 (2021)
12. G. Gui, N.J. Brooks, H.C. Kapteyn, M.M. Murnane, C.-T. Liao, Second-harmonic generation and the conservation of spatiotemporal orbital angular momentum of light. Nat. Photonics **15**(8), 608–613 (2021)
13. R. Martín-Hernández, G. Gui, L. Plaja, H.C. Kapteyn, M.M. Murnane, C.-T. Liao, M.A. Porras, C. Hernández-García, Extreme-ultraviolet spatiotemporal vortices via high harmonic generation. Nat. Photonics **19**, 817–824 (2025)
14. X. Liu, Q. Cao, N. Zhang, A. Chong, Y. Cai, Q. Zhan, Spatiotemporal optical vortices with controllable radial and azimuthal quantum numbers. Nat. Commun. **15**(1), 5435 (2024)
15. F. Feng, G. Hou, Z. Zhang, S. Ma, H. Ma, X. Li, Q. Lin, X. Zhao, M.G. Somekh, X. Yuan, Spatiotemporal optical vortex combs. Nat. Commun. **16**, 11652 (2025)
16. X. Liu, C. Liang, Q. Cao, Y. Cai, Q. Zhan, Ultrafast bursts of tailored spatiotemporal vortex pulses. Light Sci. Appl. **14**(1), 361 (2025)
17. D. Wei, B. Chen, S. Wan, Y. Wang, J. Ma, P.-Y. Wang, C. Chang, G. Qiu, Z. Tan, X. Huang et al., Nanophotonic chip-space interfaces for multidimensional nonlinear optics. Nat. Mater. **25**, 1352–1360 (2026)
18. Y. Liu, C. Lao, M. Wang, Y. Cheng, Y. Wang, S. Fu, C. Gao, J. Wang, B.B. Li, Q. Gong, Y.-F. Xiao, W. Liu, Q.-F. Yang, Integrated vortex soliton microcombs. Nat. Photonics **18**, 632–637 (2024)
19. S.W. Hancock, S. Zahedpour, A. Goffin, H.M. Milchberg, Free-space propagation of spatiotemporal optical vortices. Optica **6**(12), 1547–1553 (2019)
20. S.W. Hancock, S. Zahedpour, H.M. Milchberg, Mode structure and orbital angular momentum of spatiotemporal optical vortex pulses. Phys. Rev. Lett. **127**(19), 193901 (2021)
21. S. Derevyanko, J. Prilepsky, S. Turitsyn, Capacity estimates for optical transmission based on the nonlinear Fourier transform. Nat. Commun. **7**, 12710 (2016)
22. W. Wang, H. Liu, J. Wu, J.F. McMillan, D.I. Lee, F. Hu, W. Liu, J. Yang, H. Yang, A.K. Vinod et al., Free-space terabit/s coherent optical links via platicon frequency microcombs. eLight **5**, 8 (2025)
23. Y. Yan, G. Xie, M.P.J. Lavery, H. Huang, N. Ahmed, C. Bao, Y. Ren, Y. Cao, L. Li, Z. Zhao, A.F. Molisch, M. Tur, M.J. Padgett, A.E. Willner, High-capacity millimetre-wave communications with orbital angular momentum multiplexing. Nat. Commun. **5**, 4876 (2014)
24. L. Gong, Q. Zhao, H. Zhang, X.-Y. Hu, K. Huang, J.-M. Yang, Y.-M. Li, Optical orbital-angular-momentum-multiplexed data transmission under high scattering. Light Sci. Appl. **8**, 27 (2019)
25. S. Kotler, N. Akerman, Y. Glickman, A. Keselman, R. Ozeri, Single-ion quantum lock-in amplifier. Nature **473**, 61–65 (2011)
26. F. Krausz, M.I. Stockman, Attosecond metrology: from electron capture to future signal processing. Nat. Photonics **8**(3), 205–213 (2014)
27. Y.-C. Lin, K. Midorikawa, Y. Nabekawa, Wavefront control of subcycle vortex pulses via carrier-envelope-phase tailoring. Light Sci. Appl. **12**(1), 279 (2023)
28. S. Kim, A. Krasnok, A. Alù, Complex-frequency excitations in photonics and wave physics. Science **387**(6741), eado4128 (2025)
29. R.-J. Essiambre, G. Kramer, P.J. Winzer, G.J. Foschini, B. Goebel, Capacity limits of optical fiber networks. J. Lightwave Technol. **28**(4), 662–701 (2010)
30. S. Mittal, G. Moille, K. Srinivasan, Y.K. Chembo, M. Hafezi, Topological frequency combs and nested temporal solitons. Nat. Phys. **17**(10), 1169–1176 (2021)
31. C.J. Flower, M. Jalali Mehrabad, L. Xu, G. Moille, D.G. Suarez-Forero, O. Örsel, G. Bahl, Y. Chembo, K. Srinivasan, S. Mittal, Observation of topological frequency combs. Science **384**(6702), 1356–1361 (2024)
32. L.G. Wright, F.O. Wu, D.N. Christodoulides et al., Physics of highly multimode nonlinear optical systems. Nat. Phys. **18**, 1018–1030 (2022)
33. C. Gohle, T. Udem, M. Herrmann, J. Rauschenberger, R. Holzwarth, H.A. Schuessler, F. Krausz, T.W. Hänsch, A frequency comb in the extreme ultraviolet. Nature **436**(7048), 234–237 (2005)
34. Q.-F. Yang, Y. Hu, V. Torres-Company, K. Vahala, Efficient microresonator frequency combs. eLight **4**, 18 (2024)
35. Y. Zhao, J.K. Jang, G.J. Beals, K.J. McNulty, X. Ji, Y. Okawachi, M. Lipson, A.L. Gaeta, All-optical frequency division on-chip using a single laser. Nature **627**(8004), 546–552 (2024)
36. S.-Q. Li, X. Xu, R.M. Veetil, V. Valuckas, R. Paniagua-Domínguez, A.I. Kuznetsov, Phase-only transmissive spatial light modulator based on tunable dielectric metasurface. Science **364**(6445), 1087–1090 (2019)
37. C.L. Panuski, I. Christen, M. Minkov, C.J. Brabec, S. Trajtenberg-Mills, A.D. Griffiths, J.J.D. McKendry, G.L. Leake, D.J. Coleman, C. Tran et al., A full degree-of-freedom spatiotemporal light modulator. Nat. Photonics **16**(12), 834–842 (2022)
38. A.M. Shaltout, V.M. Shalaev, M.L. Brongersma, Spatiotemporal light control with active metasurfaces. Science **364**(6441), eaat3100 (2019)
39. P.F. McManamon, T.A. Dorschner, D.L. Corkum, L.J. Friedman, D.S. Hobbs, M. Holz, S. Liberman, H.Q. Nguyen, D.P. Resler, R.C. Sharp et al., Optical phased array technology. Proc. IEEE **84**(2), 268–298 (1996)
40. J. Sun, E. Timurdogan, A. Yaacobi, E.S. Hosseini, M.R. Watts, Large-scale nanophotonic phased array. Nature **493**(7431), 195–199 (2013)
41. J. Feldmann, N. Youngblood, M. Karpov, H. Gehring, X. Li, M. Stappers, M. Le Gallo, X. Fu, A. Lukashchuk, A.S. Raja, J. Liu, Parallel convolutional processing using an integrated photonic tensor core. Nature **589**(7840), 52–58 (2021)
42. Z. Xu, X. Yuan, T. Zhou, L. Fang, A multichannel optical computing architecture for advanced machine vision. Light Sci. Appl. **11**(1), 255 (2022)
43. Z. Xu, T. Zhou, M. Ma, C.C. Deng, Q. Dai, L. Fang, Large-scale photonic chiplet Taichi empowers 160-TOPS/W artificial general intelligence. Science **384**, 202–209 (2024)
44. Z. Zhang, L. Kong, L. Zhang, X. Pan, T. Das, B. Wang, B. Liu, F. Wang, I. Nape et al., Structured light meets machine intelligence. eLight **5**, 26 (2025)